Neurobiology of Disease 105 (2017) 164–178

Contents lists available at ScienceDirect

Neurobiology of Disease

journal homepage: www.elsevier.com/locate/ynbdi

A systems level analysis of epileptogenesis-associated proteome alterations

Michael Keck [a,1], Ganna Androsova [b,1], Fabio Gualtieri [a], Andreas Walker [a], Eva-Lotta von Rüden [a], Vera Russmann [a], Cornelia A. Deeg [c,d], Stefanie M. Hauck [e], Roland Krause [b,*], Heidrun Potschka [a,**]

[a] Institute of Pharmacology, Toxicology and Pharmacy, Ludwig-Maximilians-University (LMU), 80539 Munich, Germany
[b] Bioinformatics Core, Luxembourg Centre for Systems Biomedicine (LCSB), University of Luxembourg, 4367 Belvaux, Luxembourg
[c] Institute of Animal Physiology, Department of Veterinary Sciences, Ludwig-Maximilians-University (LMU), 80539 Munich, Germany
[d] Experimental Ophthalmology, Philipps University of Marburg, 35037 Marburg, Germany
[e] Research Unit Protein Science, Helmholtz Center Munich, 85764 Neuherberg, Germany

ARTICLE INFO

Article history:
Received 26 October 2016
Revised 22 May 2017
Accepted 29 May 2017
Available online xxxx

Keywords:
Status epilepticus
WGCNA
Epilepsy
Network
Mass spectrometry
Bioinformatics
Proteome

ABSTRACT

Despite intense research efforts, the knowledge about the mechanisms of epileptogenesis and epilepsy is still considered incomplete and limited. However, an in-depth understanding of molecular pathophysiological processes is crucial for the rational selection of innovative biomarkers and target candidates.

Here, we subjected proteomic data from different phases of a chronic rat epileptogenesis model to a comprehensive systems level analysis. Weighted Gene Co-expression Network analysis identified several modules of interconnected protein groups reflecting distinct molecular aspects of epileptogenesis in the hippocampus and the parahippocampal cortex. Characterization of these modules did not only further validate the data but also revealed regulation of molecular processes not described previously in the context of epilepsy development. The data sets also provide valuable information about temporal patterns, which should be taken into account for development of preventive strategies in particular when it comes to multi-targeting network pharmacology approaches.

In addition, principal component analysis suggests candidate biomarkers, which might inform the design of novel molecular imaging approaches aiming to predict epileptogenesis during different phases or confirm epilepsy manifestation. Further studies are necessary to distinguish between molecular alterations, which correlate with epileptogenesis versus those reflecting a mere consequence of the status epilepticus.

1. Introduction

Epilepsy is among the most common neurological disorders requiring chronic therapeutic management. Thirty percent of all patients do not respond to available anti-epileptic drugs (AEDs) (Potschka and Brodie, 2012) with a particular high rate of drug resistance in patients with acquired epilepsies. Limitations in epilepsy treatment spur a growing interest in the development of preventive approaches, which can be applied in patients who experienced an epileptogenic brain insult (Kobow et al., 2012). The design and validation of respective approaches faces several challenges. The complexity of the molecular and cellular alterations characterizing epileptogenesis following an initial brain insult renders it difficult to pick the most promising targets for anti-epileptogenic concepts in a straightforward manner. The uncertainty in the timing of epileptogenesis requires elaborate and time-consuming preclinical and clinical research (White, 2012; Schmidt, 2012). Post-insult epilepsy can develop with a latency period of months, years, or even decades (Schmidt, 2012; Trinka and Brigo, 2014). Biomarkers that allow for early conclusions about the success of an intervention and limit the necessary duration of a clinical trial are urgently needed. Brain insults only pose patient subgroups at risk for epilepsy development with the individual outcome depending on various factors including genetic and physiological factors as well as, the disease history. Stratification of patients with a comparable brain insult by an actual risk of epileptogenesis is highly desirable. For these purposes the availability of valid epileptogenesis biomarkers, which for instance render a basis for respective molecular imaging approaches, is essential. Moreover,

* Corresponding author at: Bioinformatics Core, Luxembourg Centre for Systems Biomedicine (LCSB), Université du Luxembourg, 6, avenue du Swing, L-4367 Belvaux, Luxembourg.
** Corresponding author at: Institute of Pharmacology, Toxicology, and Pharmacy, Ludwig-Maximilians-University (LMU), Koeniginstr. 16, D-80539 Munich, Germany.
E-mail addresses: roland.krause@uni.lu (R. Krause), potschka@pharmtox.vetmed.uni-muenchen.de (H. Potschka).
[1] Both authors contributed equally.
Available online on ScienceDirect (www.sciencedirect.com).

http://dx.doi.org/10.1016/j.nbd.2017.05.017

an in-depth understanding of the sequence of pathophysiological events is a prerequisite for the rationale selection of target candidates and the respective time window for intervention.

Animal models of epileptogenesis can provide information about the regulation patterns of functional groups of proteins. Bioinformatic approaches to analyze genomic, transcriptomic and proteomic data can integrate the complex data from such omics studies with the vast amount of information collected and curated in biological databases. Findings obtained can guide the selection of novel target and biomarker candidates.

Knowledge-based proteomics analysis can provide comprehensive information about disease-associated alterations in molecular patterns at the functionally relevant level and might guide the identification of key proteins in the pathogenesis of epilepsy. Therefore, we collected individual hippocampal and parahippocampal cortex samples in a rat model at three different time points during epileptogenesis and analysed the proteome alterations using an LC/MS-MS approach. Here, we completed a broader analysis of the data set previously subjected to an analysis focused on proteins specifically linked with inflammation and immune response (Walker et al., 2016). We applied a Weighted Gene Co-expression Network Analysis (WGCNA) approach (Langfelder and Horvath, 2008) to unveil a network of epileptogenesis-associated protein modules and to identify intramodular hub proteins. WGCNA has been successfully applied to discover hub gene association in many conditions including atrial fibrillation (Tan et al., 2013), Alzheimer's disease (Miller et al., 2010), Huntington's disease (Shirasaki et al., 2012), autism spectrum disorder (Huang et al., 2016), and schizophrenia (Ren et al., 2015; de Jong et al., 2012). The findings can guide future selection of promising target candidates and their rational combination in multi-targeting approaches.

To identify proteins that distinguish between groups and might serve as biomarker candidates, we have subjected the protein data sets collected during the early post-insult phase, the latency phase, and the chronic epilepsy phase to principal component analysis. The results suggest several novel proteins that are prominently regulated during epileptogenesis, and that might serve as potential target and biomarker candidates. Processed data are available as supplementary file, Cytoscape network files and R scripts are available as hosted at http://doi.org/10.5281/zenodo.438918.

2. Materials and methods

2.1. Animals

The animal experiment of this study has been carried out in accordance with the German Animal Welfare act and the EU directive 2010/63/EU as approved by the responsible government (reference number 55.2-1-54-2532-94-11). Female Sprague Dawley rats (n = 59; 200–224 g) were used in the experiment and were housed under controlled standard environmental conditions (20–24 °C, 45–65% humidity, light cycle from 7:00 a.m.–7:00 p.m.). Please note that female rats were used based on our characterization of the model (Brandt et al., 2003), which revealed a high mortality rate in male rats.

The rats were purchased from Harlan Laboratories (Udine, Italy) and were allowed to habituate to the new environmental conditions for at least one week. During the experiment every attempt was made to minimize the number of animals used in the study and to avoid any pain or discomfort.

2.2. Post-status epilepticus model

Stereotactical implantation of the combined recording and stimulation electrode into the right anterior basolateral amygdala was performed as previously described by Walker et al. (2016). With a time interval of at least six weeks post-surgery a status epilepticus (SE) was induced as described by Ongerth et al. (2014). Two days, ten days and eight weeks post SE, the rats were sacrificed and brain tissue of the hippocampus (HC) and parahippocampal cortex (PHC) was used for mass spectrometry. Animals from the eight weeks group underwent a continuous video- and EEG-monitoring (24 h per day/7 days a week over 19 days) using a combined EEG- and video-detection system as previously described by Pekcec et al. (2008). Only animals with at least one spontaneous generalized seizure were used for further analysis.

2.3. Mass spectrometry, label-free quantification and protein identification

Control (n = 5) and SE (n = 5) animals were euthanized with pentobarbital (500 mg/kg i.p.; Narcoren®, Sigma-Aldrich GmbH, Munich, Germany). Tissue preparation and LC-MS/MS analysis were performed as described previously (Walker et al., 2016). For label-free quantification and protein identification the acquired MS spectra were loaded into the Progenesis LC-MS software (Version 2.5, Nonlinear Dynamics) and label-free quantification was analysed as described by Hauck et al. (2010, 2012) and Walker et al. (2016). Briefly, only unique peptides of an identified protein were used for quantification. To measure the total cumulative normalized abundance all peptides assigned to the respective protein were summarized. Only proteins quantified with at least two peptides were included for further analysis.

2.4. Pre-processing of data

Following LC-MS/MS, the corresponding gene symbols for all quantified proteins were taken from the Ensembl database (http://www.ensembl.org/Rattus_norvegicus/; version 69; 32,971 sequences). In case a gene symbol had not been established in the rat genome annotation, the human orthologue was used. Proteins with missing values were excluded from further analysis. Expression values of each time point were arcsine-transformed, median centered and analysed by principal component analysis (PCA) implemented in R software packages "FactoMineR" (Lê et al., 2008) and "factoextra" (Kassambara, 2015). To explain variation between protein profiles of SE and control groups, the top 10 contributing proteins at the first PCA dimension were further analysed.

Differentially expressed proteins were defined as proteins with fold change ≥1.5 (up-regulated in SE samples) or fold change ≤0.67 (down-regulated in SE samples) and p-values < 0.05, estimated by empirical Bayes method in "limma" R package (Smyth, 2004).

2.5. Protein co-expression network construction and module detection

To study the correlation of protein expression profiles between different time points, further analysis comprised proteins identified at all three time points. Some identified proteins mapped to the same gene symbol; we selected the ones that had the highest number of unique peptides, which were used for quantification. Protein co-expression networks were constructed with the R package WGCNA (Weighted Gene Co-expression Network Analysis) (Langfelder and Horvath, 2008). We calculated Spearman correlation coefficient between normalized protein expression profiles and converted the correlation matrix into a weighted adjacency matrix with a soft threshold $\beta = 6$. Topological analysis by density, centralization, heterogeneity, mean clustering coefficient and mean scaled connectivity were retrieved by the function *fundamentalNetworkConcepts* of WGCNA and modules were identified by topological overlap dissimilarity measure. Topological overlap indicates the relative interconnectedness between two molecules, thus identification of modules from topological dissimilarity results in membership of proteins that have a similar expression pattern. Dynamic tree cut of the network dendrogram was performed with parameters *minClusterSize* = 20 and *deepSplit* = 2.

2.6. Hub proteins and module significance

The proteins with highest connectivity within the module were defined as intramodular hubs. Since the biological plausibility and clinical utility of hubs varies, functional enrichment of the module can further help to prioritize the hub proteins for validation. Functional enrichment was determined by Core Analysis in Ingenuity Pathways Analysis (IPA; (Racine et al., 2011)). Disease association of the hub proteins was performed in DisGeNET (Pinero et al., 2015) and IPA. DisGeNET scores represent the level of evidence for gene-disease association, based on the number and type of sources (level of curation, model organisms) and the number of publications supporting the association.

The network was exported for visualization in Cytoscape (Shannon et al., 2003), where module membership was denoted as an attribute. Module expression profiles were summarized in module eigengenes. We calculated Spearman correlation between the module eigengenes and phenotype (SE and control animals) at each time point. Student asymptotic p-values below 0.001 in at least two time points indicated significant module-phenotype relationship.

2.7. Code availability

All R packages used for MS data processing and network construction are publicly available. Data analysis codes that produce the presented results and figures were written in R (v 3.2.1) and together with Cytoscape network files can be accessed at http://doi.org/10.5281/zenodo.438918.

2.8. Immunohistochemistry

Immunohistochemistry was performed for three selected proteins to confirm the result of mass spectrometry analysis. For this purpose, animals were euthanized with an intraperitoneal injection of pentobarbital (500 mg/kg; Narcoren®, Sigma-Aldrich GmbH, Munich, Germany). Next, animals were decapitated, the brains were removed and stored in 4% paraformaldehyde in 0.1 M phosphate-buffered saline (pH 7.4) at 4 °C for three days. Serial blocks were embedded in paraffin by using an embedding workstation (Histomaster 2050/Di, Bavimed, Birkenau, Germany). Coronal sections (2 μm) were cut on a microtome (1165/Rotocut, Reichert-Jung, Nußloch, Germany) from these blocks and representative regions were selected for immunohistochemistry. For the PHC stainings (annexin A3, eukaryotic translation initiation factor 3 subunit C) we used sections close to bregma = −4.80, while for HC staining (clusterin) we used bregma = −5.40 according to the rat stereotaxic atlas (Paxinos and Watson, 2007) For all tissues we used the whole mount staining technique. Briefly, sections were initially deparaffinized with ethanol scale, processed for heat-induced epitope retrieval (HIER) with sodium citrate buffer (pH 6.0) in microwave oven at 720 W for 20 min. Samples were then washed in 0.01 M PBS at room temperature and endogenous peroxidase was inhibited for 30 min in 3% H_2O_2 in 0.01 M PBS. Tissue underwent a blocking step of 1 h in 0.01 M PBS containing 0.3% Tween-20, 2% bovine serum albumin and 5% normal donkey serum. Brain slices were then incubated overnight (16 h) with primary antibodies: i) rabbit polyclonal Anti-ANXA3 (Sigma-Aldrich Cat# HPA013398 RRID: AB_1844861) at 1:1000 dilution, ii) rabbit polyclonal Anti-Apolipoprotein J Polyclonal (Bioss Inc. Cat# bs-1354R RRID: AB_10856803) at 1:100 dilution, iii) Anti- EIF3C antibody (Biorbyt Cat# orb247746) at 1:500 dilution. The following day, after three washes in 0.01 M PBS, sections were incubated for 2 h at room temperature with biotinylated donkey anti-rabbit IgG (Jackson ImmunoResearch Labs Cat# 711-065-152 RRID:AB_2340593). Sections were then rinsed thrice in 0.01 M PBS and then incubated at room temperature for 1 h with VECTASTAIN ABC-Peroxidase Kit (Vector Laboratories Cat# PK-4000 RRID:AB_2336818) and stained using the avidin–biotin complex indirect technique (Gualtieri et al., 2012) with diaminobenzidine tablets (Sigma Aldrich, D4293 SIGMAFAST 3,3′-Diaminobenzidine tablets) as chromogen. Brain samples were then rinsed in water, dried and coverslipped with mounting medium (Millipore - 107960 Entellan) for image analysis.

2.9. Image analysis

For each animal, images for the HC or PHC were captured at 10× magnification by an Olympus BH-2 microscope connected to a video camera (Zeiss AxioCam MRc, Germany) and post processed for analysis with ImageJ software (NIH, USA) and Adobe Photoshop CS6 (Adobe Systems, USA). The person performing the quantification was unaware of the group allocation of the samples.

Images were processed for area measurement and were initially converted in 8bit type; the region of interest (ROI) for each staining was outlined. For annexin A3 we analysed the piriform cortex, for clusterin the dorsal and the ventral HC, for eukaryotic translation initiation factor 3 subunit C the amygdalopiriform transition. The threshold function was then applied to the ROI and the triangle filter (Zack et al., 1977) was chosen since this implementation uses robust (default is 1% and 99%) estimation of image histogram ends. For every image, thresholded and total ROI areas were obtained and the amount of thresholded ROI areas was normalized on the investigated area as follows:

$$\textbf{\textit{Protein marker}}\ (\textbf{\textit{normalized}}) = \textbf{\textit{thresholded area}}/\textbf{\textit{ROI area}}$$

Values obtained for each experimental group were compared between SE animals and control animals for each protein marker.

2.10. Statistical analysis

Immunhistochemistry data were analysed using Prism 5.0 (Graphpad Software, USA). Statistical analysis was performed with *t*-test. All values are expressed as mean ± SEM. For all analyses $p < 0.05$ was considered statistically significant.

3. Results

3.1. Data preprocessing

A total of 2653 proteins were detected in at least one time point by LTQ OrbitrapXL, 2241 in the HC samples and 2394 in the PHC.

In the HC, 1337 proteins were identified at all three time points and 1371 in the PHC. The overlap between the two brain regions comprises 2125 proteins and 1125 proteins after filtering by presence at all time points. After normalization, GLI pathogenesis-related 2 (Glipr2) in HC data was identified as an outlier and removed from further analysis.

Correlation between samples shows a clear separation of the third time point (Supplementary Fig. 1). Differential expression analysis of HC data indicated 121 proteins differentially expressed at two days, 276 proteins at ten days and 14 proteins at eight weeks post SE (Fig. 1a, Supplementary Fig. 2a). In the PHC 218, 419, and 223 proteins proved to be differentially expressed two days, ten days, and eight weeks post SE, respectively (Fig. 1b, Supplementary Fig. 2b). Differentially expressed proteins of all three time points exhibited an overlap of 4 proteins in the HC (Fig. 1c) and 23 proteins in the PHC (Fig. 1d). The overlap between proteins dysregulated during the early post-insult phase and the latency phase comprised 43 and 129 proteins in the HC and PHC, respectively. Three and 41 proteins exhibited a regulation during the latency phase, which extended into the chronic phase.

Comparison between brain regions revealed an overlap of 27 proteins two days post SE (Fig. 1e), 87 proteins ten days post SE (Fig. 1f) and 8 proteins eight weeks post SE (Fig. 1g) co-regulated in the HC and PHC.

The functional annotation of differentially expressed proteins revealed a typical pattern for many protein groups linked with specific biological processes (Fig. 2a (HC) and b (PHC)) and molecular function

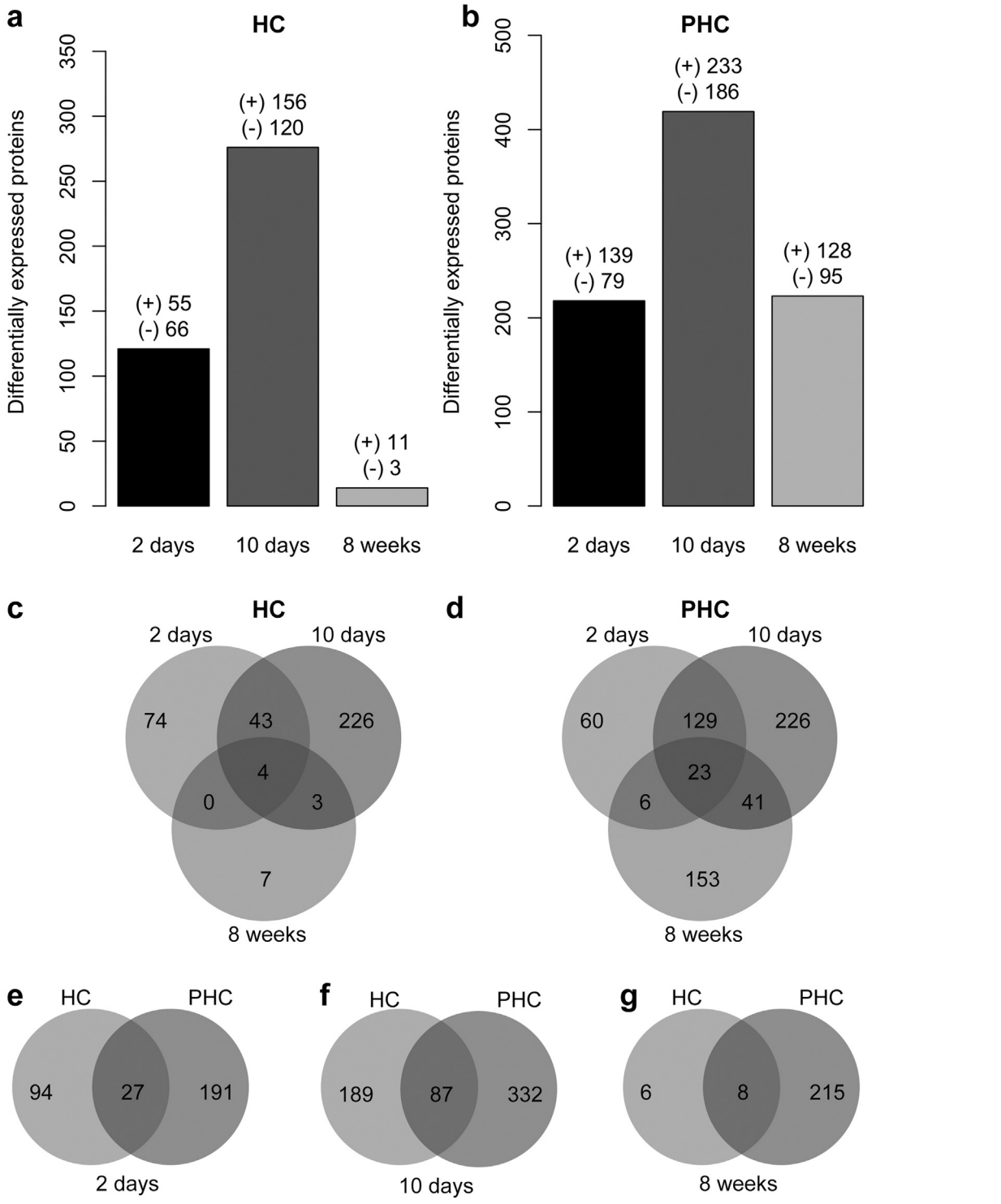

Fig. 1. Differentially expressed proteins: Differentially expressed proteins of the HC and the PHC are shown in (a and b). A positive sign (+) indicates up-regulated expression, whereas a negative sign (−) displays down-regulated expression of proteins in SE animals compared to control animals. The overlap between differentially expressed proteins of all time points is illustrated by Venn diagrams for the HC (c) and the PHC (d). (e–g) show the overlap between the two tissues (HC and PHC) two days (e), ten days (f) and eight weeks (g) post SE.

(Fig. 2c (HC) and d (PHC)) exhibiting an early dysregulation, a more pronounced regulation during the latency phase, and a reduction in the number of regulated proteins in the chronic phase. Interestingly, the same functional groups showed the most intense regulation in the HC and PHC. Regarding biological processes these included proteins associated with cellular component organization and biogenesis, cellular processes, localization and metabolic processes. Among the groups linked with a particular molecular function, proteins associated with binding, structural molecule activity, and catalytic activity stood out with prominent regulation.

3.2. HC and PHC networks and modules

Weighted co-expression networks were constructed from all proteins identified at three time points in the HC and PHC. The constructed networks had a similar topology in terms of density, heterogeneity, and

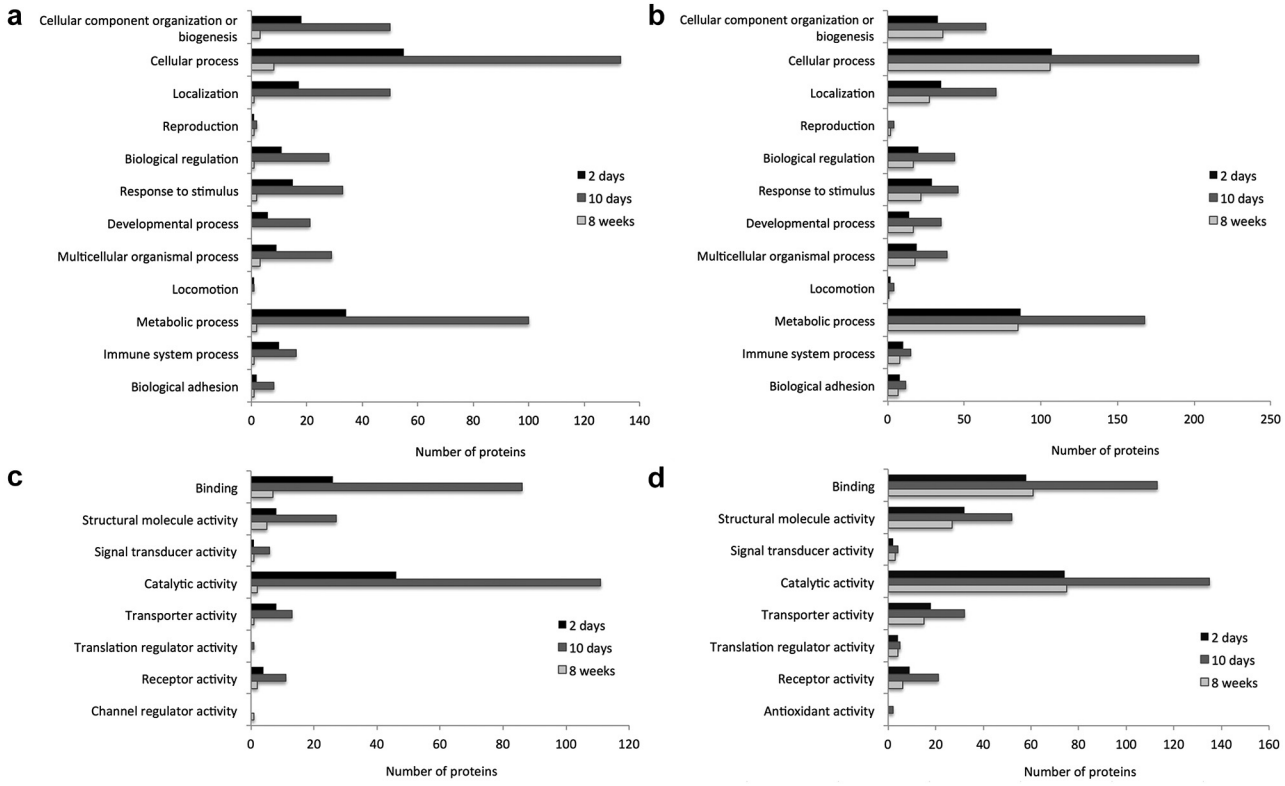

Fig. 2. Classification of differentially expressed proteins: Proteins were classified regarding biological process (a and b) and molecular function (c and d) in the HC (a and c) and the PHC (b and d).

clustering coefficient (Supplementary Table 1). Both HC and PHC networks have a free-scale topology and strong connectivity. Hierarchical clustering of protein expression profiles identified groups of co-expressed proteins (modules). Branches of the network clustered into modules were assigned a colour and a numeric value (Fig. 3a and b). Using the same criteria for module assignment HC and PHC networks contain 8 and 12 modules, respectively. Constructed networks were also visualized in Cytoscape, where node colour indicated module membership (Supplementary Fig. 3).

Jaccard similarity index indicated a high overlap between HC module 2 and PHC module 2 (Supplementary Fig. 4). Other modules with high protein membership overlap (Jaccard index ≥0.1) included HC module 1 and PHC modules 3 and 7 as well as HC module 3 and PHC module 1.

Correlation analysis of protein expression profiles of post-SE samples, indicated modules of interest for further analysis. Based on a threshold of 0.2 of protein significance we selected modules 3, 4, 6 and 7 from the HC network and modules 1, 3, 4, 7, 8 and 12 from the PHC network (Supplementary Fig. 5). Please note that the arbitrary threshold of 0.2 refers to protein significance, which describes the correlation of protein expression profiles with samples from animals with a SE history. Thus, selected modules have a minimum 20% correlation with the post-SE condition.

To further investigate the link of modules with the post-SE state, we regressed module eigengenes on SE status. Protein expression profiles of a particular module can be summarized by the first principal component, also referred to as module eigengene. We evaluated correlation between module eigengenes and the history of a SE by Spearman's rank correlation coefficient. According to our defined criteria (p-value < 0.001 for at least two time points), previously highlighted modules as well as novel ones were significantly associated with SE (Fig. 3c and d). Modules with negative correlation with the history of a SE included HC modules 3, 4, 6, 7 and PHC modules 4, 5, 7. These modules have a large number of proteins that are down-regulated in SE samples. PHC modules 3 and 8 have positive SE association at all time points, where proteins are predominantly over-expressed in SE samples. HC module 8 as well as PHC modules 1 and 12 exhibited a mixed (positive and inverse) association at different time points.

3.3. Functional enrichment and regulatory proteins

To determine functional enrichment of the modules, each module was analysed with IPA. The top 5 enriched pathways for the highlighted modules are represented in Fig. 4. Significantly enriched pathways for example included Rho family signaling (HC module 3, 4 and PHC module 3, 8), HIPPO signaling (HC module 4), 14-3-3 family signaling (HC module 4), amyloid processing (HC module 6), axonal guidance signaling (HC module 3, 6), chemokine signaling (HC module 7), gluconeogenesis (HC module 8), dopamine in cAMP signaling (PHC module 1), mitochondrial dysfunction (PHC module 3, 7, 12), mTOR signaling (PHC module 5), production of nitric oxide and reactive oxygen species in macrophages (HC module 7), and leukocyte extravasation signaling (PHC module 8). Based on the outcome of the pathway enrichment analysis we also assessed whether modules can be linked with distinct aspects of epileptogenesis. Some of the modules stand out regarding an obvious functional association of their top regulated pathways. For example HC module 4 comprises several significantly enriched pathways, which are involved in control and regulation of cell death and apoptosis as well as protein degradation. Respective pathways include HIPPO signaling, 14-3-3-mediated signaling, Myc mediated apoptosis signaling, and the protein ubiquitination pathway. HC modules 3 and 6 are characterized by the regulation of proteins playing a role in cellular plasticity (3: signaling by Rho family GTPases, RhoGDI signaling, RhoA signaling, axonal guidance signaling; 6: actin cytoskeleton signaling, epithelial adherens junction signaling, axonal guidance signaling) or being linked with other neurological diseases (Huntington's disease signaling, amyloid processing). The list of top 5 regulated pathways of HC module 8 comprises pathways, which are involved in carbohydrate and amino

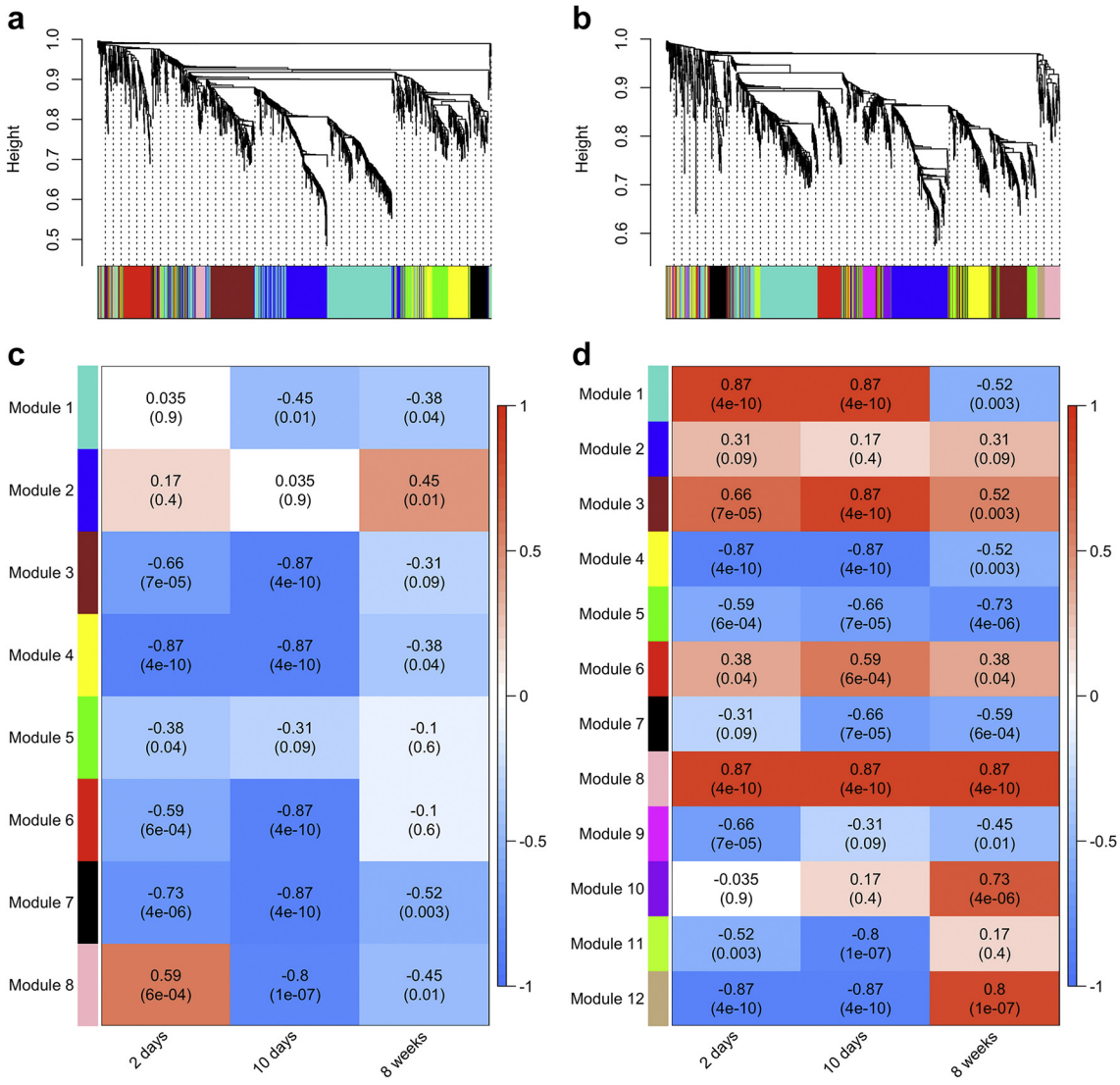

Fig. 3. WGCNA results for the HC and the PHC: Network dendrograms and module assignments are shown in (a and b). Vertical "leaves" of the dendrogram represent genes. The y-axis represents network distance, which is determined by 1–topological overlap (TO). Values closer to 1 indicate greater dissimilarity of probe expression profiles across the samples. Colour blocks below denote the module assignment determined by Dynamic Hybrid algorithm. The height cut off for dendrogram dissection into modules was determined by Dynamic Hybrid algorithm. Dendrogram constructed for the HC network (a) with height cut off 0.992 resulted in 8 modules. Dendrogram constructed for the PHC network (b) with height cut off 0.993 resulted in 12 modules. Module eigengene correlation with SE is given in (c and d). HC (c) and PHC (d) modules showed a negative correlation with SE, if proteins were under-expressed in SE samples, and a positive correlation, if proteins were over-expressed in SE samples. Spearman's rank correlation values are indicated on the top with respective Student asymptotic p-values below.

acid metabolism (gluconeogenesis 1, GDP-mannose biosynthesis, aspartate degradation II, citrulline biosynthesis, glycogen degradation).

In the PHC module 5 is characterized by enrichment of pathways linked with the regulation of cell death and apoptosis (EIF2 signaling, regulation of eIF4 and p70S6K signaling, phagosome maturation, mTOR signaling). PHC module 8 comprises pathways involved in plasticity and leukocyte transendothelial migration (signaling by Rho family GTPases, RhoA signaling, actin cytoskeleton signaling, leukocyte extravasation signaling).

Highly connected nodes of the network, often called hubs, serve as the information flow centers in the small-world, free-scale networks (Albert et al., 2000). Multiple molecular and brain networks indicated that hub targeting leads to lethal effect on the functional level (Jeong et al., 2001; Stam et al., 2007). Thus, hubs can be considered as regulatory elements of the modules. We highlighted the top 15 connected proteins within SE-associated modules and indicated their relative degree by the font size (Fig. 4). The lists of top 5 connected proteins per module were further checked for significantly regulated hub proteins. In the HC the majority of significantly regulated hub proteins proved to be down-regulated (Table 1). Only selected hippocampal hub proteins exhibited an upregulation. These included acyl-CoA dehydrogenase, long chain (HC module 4) induced during the latency phase, i.e. ten days following SE, as well as clusterin (HC module 7) induced at all time points during epileptogenesis and following epilepsy manifestation (Table 1). A higher number of hub proteins showed an overexpression in the PHC (Table 2). The list of respective proteins comprised eukaryotic translation initiation factor 3 subunit C (PHC module 1; two and ten days post SE), ribosomal protein L30 (PHC module 4; two and ten days post SE), and synaptotagmin binding, cytoplasmic RNA interacting protein (PHC module 4; two and ten days post SE). In PHC module 5 four of the top 5 hub proteins exhibited an upregulation in the course of epileptogenesis and epilepsy manifestation: opioid binding protein/cell adhesion molecule like (ten days post SE), integrin subunit beta 1 (two and ten days and eight weeks post SE), integrin subunit alpha 6 (two and ten days and eight weeks post SE), and neuronal growth regulator 1 (ten days post SE). All top 5 hub proteins of PHC module 8 proved to be significantly induced with one protein regulated ten days post SE (nicotinamide nucleotide transhydrogenase), one protein

HC Module 3

IPA Canonical Pathways	-log(p-value)
Signaling by Rho Family GTPases	8.83
RhoGDI Signaling	8.73
RhoA Signaling	7.46
Lipid Antigen Presentation by CD1	6.78
Axonal Guidance Signaling	6.5

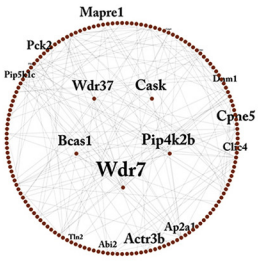

PHC Module 3

IPA Canonical Pathways	-log(p-value)
Clathrin-mediated Endocytosis Signaling	14.8
Mitochondrial Dysfunction	12.1
Remodeling of Epithelial Adherens Junctions	7.74
TCA Cycle II (Eukaryotic)	7.18
Signaling by Rho Family GTPases	6.32

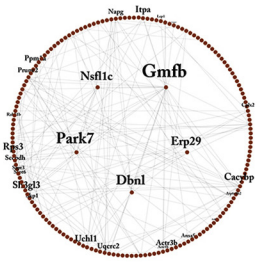

HC Module 4

IPA Canonical Pathways	-log(p-value)
HIPPO signaling	9.1
14-3-3-mediated Signaling	7.78
Protein Ubiquitination Pathway	7.24
Signaling by Rho Family GTPases	6.75
Myc Mediated Apoptosis Signaling	6.64

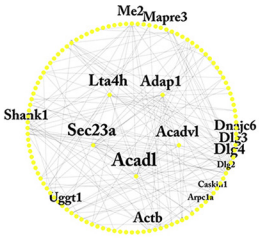

PHC Module 4

IPA Canonical Pathways	-log(p-value)
Melatonin Signaling	9.2
Nitric Oxide Signaling in the Cardiovascular System	9.07
Molecular Mechanisms of Cancer	8.8
Role of NFAT in Cardiac Hypertrophy	8.76
Breast Cancer Regulation by Stathmin1	8.44

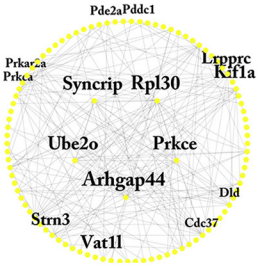

HC Module 6

IPA Canonical Pathways	-log(p-value)
Actin Cytoskeleton Signaling	5.25
Epithelial Adherens Junction Signaling	4.31
Huntington's Disease Signaling	4.12
Amyloid Processing	4.1
Axonal Guidance Signaling	3.86

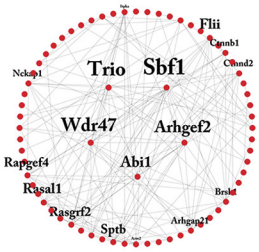

PHC Module 5

IPA Canonical Pathways	-log(p-value)
EIF2 Signaling	6.14
Regulation of eIF4 and p70S6K Signaling	3.84
phagosome maturation	3.3
mTOR Signaling	3.26
D-myo-inositol (1,4,5,6)-Tetrakisphosphate Biosynthesis	3.16

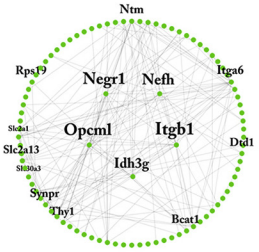

HC Module 7

IPA Canonical Pathways	-log(p-value)
Cholecystokinin/Gastrin-mediated Signaling	3.23
Gαq Signaling	2.63
Chemokine Signaling	2.6
PAK Signaling	2.33
Production of Nitric Oxide and Reactive Oxygen Species in Macrophages	2.31

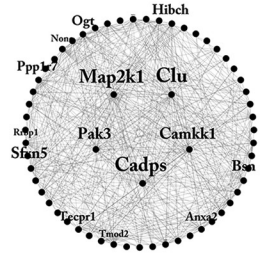

PHC Module 7

IPA Canonical Pathways	-log(p-value)
Mitochondrial Dysfunction	11.8
Oxidative Phosphorylation	9.12
Clathrin-mediated Endocytosis Signaling	3.75
Sucrose Degradation V (Mammalian)	3.55
phagosome maturation	3.43

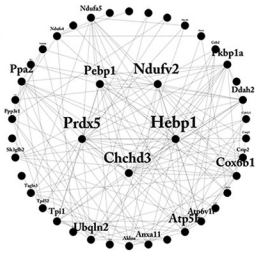

HC Module 8

IPA Canonical Pathways	-log(p-value)
Gluconeogenesis I	4.59
GDP-mannose Biosynthesis	4.11
Aspartate Degradation II	3.97
Citrulline Biosynthesis	3.84
Glycogen Degradation II	3.55

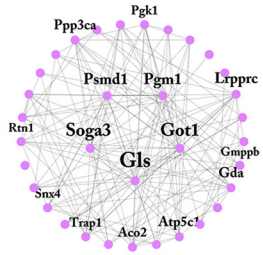

PHC Module 8

IPA Canonical Pathways	-log(p-value)
Signaling by Rho Family GTPases	6.52
RhoA Signaling	5.91
Actin Cytoskeleton Signaling	4.48
Fatty Acid β-oxidation I	4
Leukocyte Extravasation Signaling	3.61

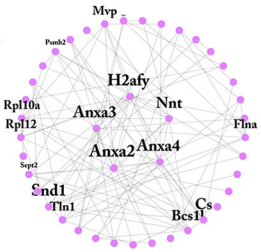

PHC Module 1

IPA Canonical Pathways	-log(p-value)
Dopamine-DARPP32 Feedback in cAMP Signaling	7.37
p70S6K Signaling	7.11
Synaptic Long Term Depression	5.42
Protein Kinase A Signaling	5.23
Role of NFAT in Cardiac Hypertrophy	5.21

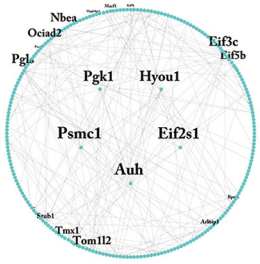

PHC Module 12

IPA Canonical Pathways	-log(p-value)
IGF-1 Signaling	8.33
Mitochondrial Dysfunction	6.85
ERK/MAPK Signaling	6.62
Oxidative Phosphorylation	6.34
Cell Cycle: G2/M DNA Damage Checkpoint Regulation	6.15

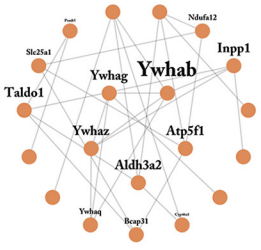

Fig. 4. Functional enrichment of modules and intramodular hubs: Tables list the top 5 canonical pathways identified by IPA. Figures present the top 150 protein connections within each module. The labeled nodes denote the top 15 intramodular hubs in the module. Protein name size is proportional to the relative degree of the node within the respective module. Node colour reflects the previously assigned module membership in the network dendrogram.

regulated ten days and eight weeks post SE (annexin A3) and the other hub proteins being regulated at all time points (annexin A2, H2A histone family member Y, and annexin A4).

Hub-disease association was queried in OMIM (Hamosh et al., 2005), IPA and DisGeNET databases. All significantly up-regulated hubs had an associated OMIM term. DisGeNET indicated a strong association

Table 1
Top 5 intramodular hubs for modules in the HC.

Gene symbol	Protein	Connectivity[a]	p-Value[b]	Fold change[b]	p-Value[b]	Fold change[b]	p-Value[b]	Fold change[b]
			2 days post SE		10 days post SE		8 weeks post SE	
Module 3								
Wdr7	WD repeat domain 7	1.000	0.048	0.81	0.006	0.68	0.952	0.99
Wdr37	WD repeat domain 37	0.916	0.248	0.87	0.059	0.78	0.907	0.99
Pck2	Phosphoenolpyruvate carboxykinase 2 (mitochondrial)	0.904	0.709	0.95	0.005	0.68	0.254	0.90
Pip5k1c	Phosphatidylinositol-4-phosphate 5-kinase type 1 gamma	0.888	0.064	0.82	0.001	0.62	0.329	0.90
Cpne5	Copine 5	0.885	0.025	0.78	0.012	0.67	0.112	0.87
Module 4								
Acadl	Acyl-CoA dehydrogenase, long chain	1.000	0.022	1.32	0.006	1.51	0.538	1.05
Sec23a	Sec23 homolog A, coat complex II component	0.924	0.000	0.37	0.000	0.35	0.833	0.97
Lta4h	Leukotriene A4 hydrolase	0.919	0.010	1.41	0.082	1.27	0.291	1.08
Dlg4	Discs large MAGUK scaffold protein 4	0.917	0.045	0.83	0.002	0.66	0.155	0.87
Adap1	ArfGAP with dual PH domains 1	0.858	0.014	0.74	0.023	0.75	0.151	0.85
Module 6								
Sbf1	SET binding factor 1	1.000	0.023	0.78	0.018	0.77	0.884	1.04
Wdr47	WD repeat domain 47	0.931	0.013	0.75	0.006	0.63	0.919	1.02
Trio	Trio Rho guanine nucleotide exchange factor	0.845	0.001	0.59	0.003	0.51	0.835	1.10
Rasal1	RAS protein activator like 1 (GAP1 like)	0.835	0.027	0.69	0.001	0.59	0.873	0.97
Scai	Suppressor of cancer cell invasion	0.813	0.150	0.80	0.032	0.66	0.644	0.93
Module 7								
Map2k1	Mitogen activated protein kinase kinase 1	1.000	0.041	0.76	0.004	0.68	0.662	0.95
Clu	Clusterin	0.987	0.001	2.86	0.003	5.14	0.037	2.06
Cadps	Calcium dependent secretion activator	0.953	0.335	0.92	0.006	0.69	0.242	0.82
Camkk1	Calcium/calmodulin-dependent protein kinase kinase 1	0.882	0.037	0.70	0.009	0.57	0.704	0.95
Pak3	P21 (RAC1) activated kinase 3	0.874	0.598	0.95	0.021	0.69	0.250	0.85
Module 8								
Gls	Glutaminase	1.000	0.339	1.09	0.026	0.75	0.101	0.87
Got1	Glutamic-oxaloacetic transaminase 1	0.884	0.511	1.06	0.011	0.80	0.347	0.94
Soga3	SOGA family member 3	0.852	0.500	1.07	0.010	0.78	0.751	0.97
Ppp3ca	Protein phosphatase 3 catalytic subunit alpha	0.805	0.793	1.03	0.022	0.73	0.306	0.90
Psmd1	Proteasome 26S subunit, non-ATPase 1	0.782	0.256	1.13	0.294	0.91	0.942	1.00

[a] Proteins with highest connectivity within the module were defined as intramodular hubs.
[b] Differentially expressed proteins were defined as proteins with fold change ≥1.5 (up-regulated in SE samples) or fold change ≤0.67 (down-regulated in SE samples) and p-values < 0.05.

between Alzheimer's disease and clusterin (score = 0.29). Lower DisGeNET scores of 0.12 were observed between Amyotrophic Lateral Sclerosis and clusterin as well as opioid binding protein/cell adhesion, between Schizophrenia and integrin subunit alpha 6, between Parkinson's Disease and transaldolase 1, and between Spinocerebellar Ataxia and hypoxia up-regulated 1 (Fig. 5).

The association of hub proteins with neurological diseases is represented in Supplementary Fig. 6.

We analysed data sets of earlier epilepsy-related proteomics and transcriptomics studies, testing whether hub proteins that we identified have been demonstrated to be regulated in respective studies. The results are listed in Supplementary Table 2. A differential expression of some of the hub proteins has been described earlier. For example an induction of clusterin has been reported by Lee et al. (2007) and Hansen et al. (2014).

Additionally, we compared the molecular processes identified by our study with available data sets from transcriptomic studies. This comparison indicated a regulation of similar processes in several studies. Gorter et al. (2006) detected similar changes and major categories of processes with a regulation of apoptosis and cell death as well as plasticity associated molecular processes. Okamoto et al. (2010) demonstrated an up-regulation of the expression of genes linked with extracellular matrix remodelling and cell motility, signaling cascades, apoptosis or immune response. He et al. (2014) carried out an in-depth analysis of the dataset generated by Niesen et al. (2013). They reported a regulation of metabolism – associated pathways. In our study we identified module 8 in the HC data sets, which was functionally dominated by pathways involved in cellular metabolism.

In general, it needs to be taken into account that comparison of different data sets faces major limitations related to different study approaches including time of sampling and different techniques a direct comparison between studies is biased. When comparing data for different brain regions across studies, these are of course often contrasting. For instance, in a transcriptomic analysis a hippocampal down- regulation of H2A histone family, member Y has been described which persisted during epileptogenesis (Hansen et al., 2014) We observed an induction for this protein at all analysed time points in the PHC.

3.4. In-silico result validation

To validate the identified hubs and functional modules, we additionally analysed the proteomic data set provided by Bitsika et al. (2016). The main differences between our and Bitsika's data set were the model organism (rat vs. mouse), SE induction (electrical vs. kainic acid (KA)) and the measured time points (two days, ten days and eight weeks vs. one, three and 30 days). Despite the great differences between data sets, the same supporting findings will indicate that the results are robust across organisms and SE models. In the following we refer to our present data sets as HC and PHC.

Briefly, the Bitsika data set underwent the same preprocessing and network construction steps. Among initial 1715 proteins identified at all three time points, 1326 of these proteins overlapped with HC proteins and 1351 with PHC proteins. From initial 1715 proteins identified at different time points, we retained only 1045 proteins that were present at all time points. Hippocampal data from both studies were compared regarding time course patterns (Supplementary Fig. 7a). The strongest differentially expressed protein overlaps were identified for Bitsika 1 day vs. HC 10 days (14 proteins), Bitsika 3 days vs. HC 10 days (18 proteins), and Bitsika 30 days vs. HC 10 days (41 proteins). Identified differentially expressed proteins (Supplementary Fig. 7b) had the same ratio as in the original publication: lowest number of differentially expressed proteins at day 1 (53), a larger number of differentially

Table 2
Top 5 intramodular hubs for modules in the PHC.

Gene symbol	Protein	Connectivity[a]	p-Value[b]	Fold change[b]	p-Value[b]	Fold change[b]	p-Value[b]	Fold change[b]
			2 days post SE		10 days post SE		8 weeks post SE	
Module 1								
Pgk1	Phosphoglycerate kinase 1	1.000	0.066	0.88	0.004	0.76	0.491	0.92
Eif3c	Eukaryotic translation initiation factor 3 subunit C	0.984	0.002	2.33	0.002	2.92	0.186	0.83
Psmc1	Proteasome 26S subunit, ATPase 1	0.972	0.011	0.77	0.005	0.74	0.125	1.12
Auh	AU RNA binding methylglutaconyl-CoA hydratase	0.952	0.012	1.34	0.008	1.39	0.161	0.84
Hyou1	Hypoxia up-regulated 1	0.948	0.004	0.72	0.004	0.66	0.001	1.52
Module 3								
Gmfb	Glia maturation factor, beta	1.000	0.029	0.42	0.000	0.24	0.025	0.62
Park7	Parkinsonism associated deglycase	0.896	0.035	0.59	0.000	0.38	0.100	0.85
Dbnl	Drebrin-like	0.878	0.091	0.64	0.037	0.56	0.022	0.65
Uchl1	Ubiquitin C-terminal hydrolase L1	0.849	0.420	0.81	0.016	0.48	0.008	0.72
Nsfl1c	NSFL1 cofactor	0.843	0.125	0.64	0.001	0.39	0.831	1.03
Module 4								
Arhgap44	Rho GTPase activating protein 44	1.000	0.001	0.65	0.000	0.63	0.380	0.91
Rpl30	Ribosomal protein L30	0.991	0.000	1.87	0.000	1.88	0.650	0.94
Prkce	Protein kinase C, epsilon	0.965	0.001	0.66	0.000	0.65	0.237	0.86
Syncrip	Synaptotagmin binding, cytoplasmic RNA interacting protein	0.946	0.002	1.77	0.009	1.90	0.121	1.15
Ube2o	Ubiquitin-conjugating enzyme E2O	0.944	0.000	0.53	0.001	0.50	0.011	0.76
Module 5								
Opcml	Opioid binding protein/cell adhesion molecule-like	1.000	0.176	1.22	0.036	1.58	0.025	1.29
Itgb1	Integrin subunit beta 1	1.000	0.008	1.62	0.000	2.41	0.000	2.16
Itga6	Integrin subunit alpha 6	0.961	0.099	1.64	0.000	3.32	0.000	2.17
Negr1	Neuronal growth regulator 1	0.931	0.159	1.29	0.009	1.73	0.073	1.32
Nefh	Neurofilament, heavy polypeptide	0.929	0.075	0.69	0.002	0.35	0.515	0.89
Module 7								
Hebp1	Heme binding protein 1	1.000	0.059	0.47	0.001	0.22	0.013	0.42
Prdx5	Peroxiredoxin 5	0.983	0.089	0.71	0.003	0.47	0.208	0.82
Chchd3	Coiled-coil-helix-coiled-coil-helix domain containing 3	0.924	0.261	0.75	0.004	0.48	0.044	0.57
Ndufv2	NADH:ubiquinone oxidoreductase core subunit V2	0.897	0.511	0.76	0.004	0.36	0.217	0.55
Atp5h	ATP synthase, H+ transporting, mitochondrial Fo complex, subunit d	0.890	0.930	0.97	0.030	0.53	0.006	0.44
Module 8								
Anxa2	Annexin A2	1.000	0.000	3.16	0.000	4.54	0.000	3.11
Anxa3	Annexin A3	0.960	0.060	1.60	0.000	10.38	0.000	2.59
H2afy	H2A histone family, member Y	0.953	0.005	1.58	0.000	3.01	0.005	2.03
Nnt	Nicotinamide nucleotide transhydrogenase	0.916	0.023	1.27	0.009	1.51	0.022	1.26
Anxa4	Annexin A4	0.882	0.003	1.74	0.000	3.33	0.000	1.93
Module 12								
Ywhab	14-3-3 protein beta-subtype	1.000	0.001	0.71	0.001	0.65	0.809	0.98
Prkar1b	Protein kinase cAMP-dependent type 1 regulatory subunit beta	0.925	0.001	0.60	0.000	0.50	0.179	1.21
Oxsm	3-oxoacyl-ACP synthase, mitochondrial	0.895	0.001	0.64	0.002	0.60	0.015	1.29
Taldo1	Transaldolase 1	0.888	0.000	1.56	0.001	1.51	0.049	0.84
Ywhag	14-3-3 protein gamma	0.865	0.002	0.73	0.002	0.66	0.808	0.98

[a] Proteins with highest connectivity within the module were defined as intramodular hubs.
[b] Differentially expressed proteins were defined as proteins with fold change ≥1.5 (up-regulated in SE samples) or fold change ≤0.67 (down-regulated in SE samples) and p-values < 0.05.

expressed proteins at day 3 (73) and the greatest number of differentially expressed proteins at the last time point (250). Spearman's correlation matrix showed a higher correlation between KA-samples and controls at three days as well as KA-samples at 30 days (Supplementary Fig. 7c).

Topological overlap dissimilarity identified eleven modules in the Bitsika network (Supplementary Fig. 7d) with size ranging from 48 to 198 proteins. Protein significance >0.2 and module eigengene trait-correlation (p-value < 0.001) highlighted the Bitsika modules 3, 4, 5, 10 and 11 (Supplementary Fig. 7e and f). These modules were enriched in mitochondrial dysfunction (module 3 p-value = 7.18e−14, module 10 p-value = 6.92e−07), in melatonin and cancer signaling (module 4 p-value = 6.17e−10, module 11 p-value = 1.3e−05), and in EIF2 signaling (module 5 p-value = 1.05e−06).

Next, we compared if some hub proteins from our data set also appeared as hubs in Bitsika modules. Several hub proteins including bassoon (presynaptic cytomatrix protein) (HC 7, Bitsika 10), clusterin (HC 7, Bitsika 4), heat shock protein 4-like (PHC 1, Bitsika 7), myosin XVIIIa (HC 5, Bitsika 9) and 14–3-3 protein theta (PHC 12, Bitsika 2) exhibited an overlap between modules from the two studies.

3.5. Principal component analysis (PCA)

The analysis of PCA data was focused on dimension 1 (principal component 1), which by definition exhibits the largest variation between groups under comparison. It is interesting to note that there is an obvious clustering of the subgroup's HC data along dimension 1 two and ten days but not eight weeks post SE. In contrast, clustering of PHC data is evident at all three time points (Fig. 6).

Among top 10 proteins that contribute to variability of principal component 1 (PC1), there are some that exhibit a high fold change (Tables 3 and 4). In accordance with our aim to identify interesting biomarker candidates of epileptogenesis and early epilepsy onset we have searched these lists for proteins with an upregulation of at least 1.5 fold. In the early post insult phase (two days post SE) three proteins contributing to PC1 variability exhibited a strong induction. These included

Fig. 5. Up-regulated hubs association with diseases in DisGeNET database: For visualization purpose, we included only associations with DisGeNET score above 0.1.

CD151 molecule, mannose-P-dochilol utilization defect 1 protein and clusterin. During the latency phase (ten days post SE) ectonucleoside triphosphate diphosphohydrolase 1 and plexin B2 proved to be up-regulated among the PC1 top 10 proteins. In the PHC only one PC1 top 10 protein exhibited a significant induction ten days post SE. In the chronic phase following epilepsy manifestation, four proteins of the PC1 top 10 list showed an overexpression: ATP synthase, H^+ transporting mitochondrial Fo complex, subunit F2; glutathione S-transferase alpha; proteasome subunit beta type 3; purine nucleoside phosphorylase.

3.6. Immunohistochemistry

For validation purposes we selected three proteins for immunohistochemistry based on the results of the network analysis and PCA.

Ten days following SE an increased expression of eukaryotic translation initiation factor 3 subunit C was evident in the PHC of animals with SE. The difference was most pronounced in the amygdalopiriform transition. Animals with SE exhibited small immunopositive cells in this region that were not present in control animals (Supplementary Fig. 8a and b). The immunopositive area proved to be increased by 1.5-fold (Supplementary Fig. 8c: two-sample $t(8) = 5.011$, $p = 0.001$) in animals following SE (2.496 ± 0.097 n = 5) as compared to control animals (1.628 ± 0.144 n = 5).

Ten days following SE, we confirmed an increase of annexin A3 expression in the PHC by immunohistochemistry. All animals with SE exhibited a marked difference in cell morphology in the piriform cortex, particularly in layer II (pyramidal layer). Swollen immunopositive cells that appeared densely packed were observed in animals following SE, but not in control animals (Supplementary Fig. 8d and e). Despite the pronounced variability among the SE animals, a significant 2.2-fold change in annexin A3 positive area (Supplementary Fig. 8f: two-Welch $t(6) = 2.806$, $p = 0.0309$) was demonstrated when comparing animals with SE (0.229 ± 0.044 n = 7) and control animals (0.104 ± 0.010 n = 6).

As a consequence of SE an increased expression of clusterin was confirmed in the HC. Two days following SE a trend towards an increased clusterin expression was evident in the CA1 stratum lacunosum moleculare of the dorsal HC (Supplementary Fig. 8g–i: two-sample $t(12) = 1.861$, $p = 0.087$, SE 0.049 ± 0.004 n = 7, control 0.039 ± 0.004 n = 7).

In the ventral HC (Supplementary Fig. 8j and k), clusterin was significantly upregulated in the CA3 radiatum and lacunosum moleculare layers (Supplementary Fig. 8l: two-sample $t(9) = 2.887$, $p = 0.0180$). Animals with SE (0.055 ± 0.005 n = 6) displayed a 1.7-fold increase in the area labeled for clusterin as compared to control animals (0.034 ± 0.005 n = 5).

4. Discussion

To our knowledge, this study presents the first comprehensive WGCNA-based systems biology analysis, which provides an in-depth

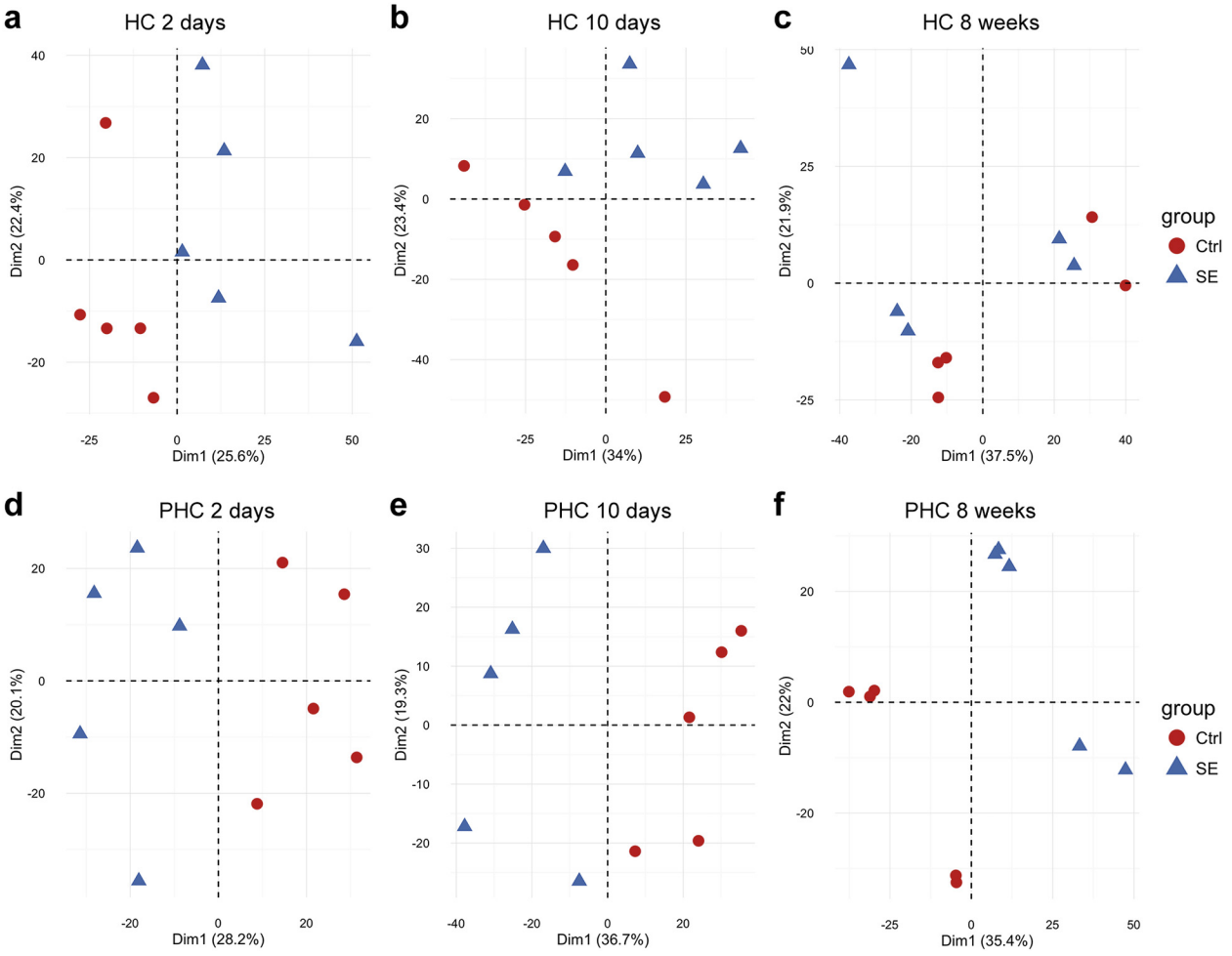

Fig. 6. Principal Component Analysis (PCA): PCA of control (Ctrl; dots) and SE animals (triangles) performed for each time point (two days, ten days and eight weeks post SE) in the HC and the PHC with all identified proteins at the specific time point as input. (a) HC two days post SE, (b) HC ten days post SE, (c) HC eight weeks post SE, (d) PHC two days post SE, (e) PHC ten days post SE, and (f) PHC eight weeks post SE.

characterization of the epileptogenesis-associated proteomic network alterations. A broad functional annotation analysis revealed a pronounced regulation of several functional groups of proteins. Both, in the HC and PHC the most prominent molecular alterations in the respective groups were evident during the latency phase, i.e. ten days following the epileptogenic brain insult. This time course seems to reflect the alterations at the cellular and network level, which of course require a high intensity of molecular processes. Thus, it is not surprising that the groups exhibiting the most pronounced regulation including several protein groups, which play a key role in synaptic and cellular plasticity and network reorganization.

The time course pattern of the regulation of functional protein groups points to another interesting aspect. There is an ongoing discussion to what extent pathophysiological mechanisms during epileptogenesis overlap with those in the early phase following epilepsy manifestation and progression phases (Dudek and Staley, 2011). Our findings indicate that some of the molecular pathological processes extend into the chronic phase with spontaneous recurrent seizures. However, the degree of their regulation is reduced to lower levels with a smaller number of proteins being regulated per functional group.

Systems biology approaches and network analyses of omics-data sets can render an important information basis for network pharmacology approaches with multi-targeting strategies or targeting of key transcription factors (Margineanu, 2016; Benson, 2015; Haanstra and Bakker, 2015). Löscher et al. (2013) have emphasized that there is an urgent need in the epileptology field for a gain-in-knowledge rendering rational design of multi-targeting approaches and drug cocktails possible. In line with these concepts we now applied a WGCNA resulting in the identification of several modules of interconnected protein groups, which reflect distinct molecular aspects of epileptogenesis in the electrical post-SE model in rats. In order to assess the robustness of the findings we included another data set recently published by (Bitsika et al., 2016) from a chemical mouse post-SE model in a direct comparative analysis.

The functional association of significantly enriched pathways characterizing the identified modules points to key pathophysiological mechanisms. It is a well-known fact that epileptogenic brain insults trigger neuronal damage and loss (Pitkänen et al., 2002). HC module 4 proved to be characterized by the regulation of molecular signaling pathways that are critically involved in the regulation of cell death and apoptosis. Whereas altered 14–3-3 signaling has previously been discussed in the context of temporal lobe epilepsy (Schindler et al., 2006), there has been only limited or no information available about the role of Myc mediated apoptosis signaling, HIPPO signaling, and protein ubiquitination during epileptogenesis. HIPPO signaling is known to play a crucial role in the regulation of cell proliferation and apoptosis (Cairns et al., 2017) as well as in tumorigenesis (Zhang et al., 2016). In addition, a link has been described between HIPPO signaling and 14-3-3 proteins (Ren et al., 2010).

The involvement of further pathways was evident in PHC module 5. Among these, mTOR signaling was repeatedly described to be modulated during epileptogenesis and in the epileptic brain (Vezzani, 2012;

Table 3
PCA for HC: top 10 contributing proteins to dimension 1.

Gene symbol	Protein	p-Value[a]	Fold change[a]
2 days post SE			
Cd151	CD151 molecule (Raph blood group)	0.016	1.89
Gprc5b	G protein-coupled receptor, class C, group 5, member B	0.052	1.61
Slc25a4	Solute carrier family 25 member 4	0.074	1.23
Mpdu1	Mannose-P-dolichol utilization defect 1	0.000	1.73
Slc25a3	Solute carrier family 25 member 3	0.340	1.12
Sfxn3	Sideroflexin 3	0.099	1.17
Lamp1	Lysosomal-associated membrane protein 1	0.085	1.36
Clu	Clusterin	0.001	2.86
Acadvl	Acyl-CoA dehydrogenase, very long chain	0.069	1.53
Mpc2	Mitochondrial pyruvate carrier 2	0.877	1.01
10 days post SE			
Itgb1	Integrin subunit beta 1	0.054	2.39
Itga6	Integrin subunit alpha 6	0.054	2.75
Nnt	Nicotinamide nucleotide transhydrogenase	0.831	1.02
Hspc159	Galectin-like	0.044	0.51
Entpd1	Ectonucleoside triphosphate diphosphohydrolase 1	0.029	2.70
Cd48	CD48 molecule	0.111	6.15
Bsn	Bassoon (presynaptic cytomatrix protein)	0.026	0.53
Slc5a3	Solute carrier family 5 member 3	0.054	2.28
Hebp1	Heme binding protein 1	0.051	0.49
Plxnb2	Plexin B2	0.021	2.44
8 weeks post SE			
Myh9	Myosin, heavy chain 9, non-muscle	0.518	1.32
Plec	Plectin	0.510	1.28
Tmod1	Tropomodulin 1	0.351	1.26
Ctnnd2	Catenin delta 2	0.481	1.22
Ablim2	Actin binding LIM protein family, member 2	0.563	1.23
Pea15	Phosphoprotein enriched in astrocytes 15	0.375	0.78
Myh10	Myosin, heavy chain 10, non-muscle	0.550	1.30
Dnaja1	DnaJ heat shock protein family (Hsp40) member A1;	0.628	1.14
Wdr48	WD repeat domain 48	0.375	1.15
Myo18a	Myosin XVIIIa	0.615	1.12

[a] Differentially expressed proteins were defined as proteins with fold change ≥1.5 (up-regulated in SE samples) or fold change ≤0.67 (down-regulated in SE samples) and p-values < 0.05.

Table 4
PCA for PHC: top 10 contributing proteins to dimension 1.

Gene symbol	Protein	p-Value[a]	Fold change[a]
2 days post SE			
Cyp46a1	Cytochrome P450, family 46, subfamily a, polypeptide 1	0.000	0.44
Abr	Active BCR-related	0.001	0.69
Inpp1	Inositol polyphosphate-1-phosphatase	0.000	0.60
Brsk2	BR serine/threonine kinase 2	0.000	0.59
Ywhah	14-3-3 protein eta	0.001	0.75
Wars	Tryptophanyl-tRNA synthetase	0.003	0.78
Strn3	Striatin 3	0.001	0.58
Oxsm	3-oxoacyl-ACP synthase, mitochondrial	0.001	0.64
Esd	Esterase D	0.004	0.80
Actbl2	Actin, beta-like 2	0.000	0.50
10 days post SE			
Ywhab	14-3-3 protein beta-subtype	0.001	0.65
Hspa4l	Heat shock protein 4-like	0.003	0.78
Strn4	Striatin 4	0.000	0.47
Ywhae	14-3-3 epsilon	0.003	0.75
Anxa3	Annexin A3	0.000	10.38
Pgls	6-Phosphogluconolactonase	0.000	0.51
Park7	Parkinsonism associated deglycase	0.000	0.38
Aco1	Aconitase 1	0.001	0.69
Esd	Esterase D	0.002	0.75
Ywhaq	14-3-3 protein theta	0.001	0.66
8 weeks post SE			
Agk	Acylglycerol kinase	0.148	1.15
Got2	Glutamic-oxaloacetic transaminase 2	0.243	1.12
Ogdh	Oxoglutarate dehydrogenase	0.143	1.19
Atp5j2	ATP synthase, H+ transporting, mitochondrial Fo complex, subunit F2	0.002	1.71
Atp5a1	ATP synthase, H+ transporting, mitochondrial F1 complex, alpha subunit 1, cardiac muscle	0.240	1.10
Gsta1	Glutathione S-transferase alpha 1	0.011	1.62
Psmb3	Proteasome subunit beta 3	0.005	1.73
Trap1	TNF receptor-associated protein 1	0.084	1.17
Pnp	Purine nucleoside phosphorylase	0.027	1.55
Ddb1	Damage-specific DNA binding protein 1	0.060	1.24

[a] Differentially expressed proteins were defined as proteins with fold change ≥1.5 (up-regulated in SE samples) or fold change ≤0.67 (down-regulated in SE samples) and p-values < 0.05.

Galanopoulou et al., 2012). In apparent contrast, there has been a lack of robust information about epileptogenesis- or epilepsy-associated regulation of signaling pathways linked with eukaryotic initiation factor and ribosomal protein S6 kinase beta-1 signaling. These pathways are associated with protein synthesis and macroautophagy and a role of these pathways has been discussed in the context of Parkinson's disease (Dijkstra et al., 2015). Respective pathways might comprise interesting target candidates for neuroprotective approaches.

Cellular plasticity constitutes one of the hallmarks of the development of temporal lobe epilepsy following an initial brain insult (Jessberger and Parent, 2015). Two of the HC modules (module 3 and 6) and one of the PHC modules (module 8) stood out with a regulation of pathways linked with cytoskeletal dynamics, cell-cell interaction, and axonal guidance. The identification of these pathways provides important molecular information for future development of innovative approaches interfering with the generation of a hyperexcitable cellular network. In the PHC, proteins associated with leukocyte extravasation signaling exhibited an intense regulation. Recently, we have already discussed respective molecular alterations and their implications in detail (Walker et al., 2016). In this previous publication, we have completed a bioinformatics analysis focused on inflammation and immunity-associated pathways. Despite the fact that some of the respective pathways were also key components of those network modules, which proved to be regulated following SE, the number of hub proteins and regulated module pathways linked with inflammation is relatively low. This might be related to a role of inflammation-associated proteins as crucial effector proteins rather than key regulatory proteins.

Moreover, assessment of regulated pathways characterizing HC module 6 pointed to a molecular overlap with pathophysiological mechanisms of other neurological diseases. The comparison of the neurobiology of Alzheimer's disease and epilepsy has already been a focus of experimental and clinical studies (Noebels, 2011; Chin and Scharfman, 2013). In contrast, the mechanistic link between Huntington's disease and epilepsy suggested by our findings needs to be further explored.

In general, it is of interest that several hub proteins of different modules have already been linked with various neurological and psychiatric diseases (Fig. 5). Among these hub proteins annexin A2, clusterin, and integrin subunit beta 1 are standing out exhibiting a link with multiple diseases.

The regulation of HC module 8 pathways linked with carbohydrate and amino acid metabolism might reflect a general metabolic dysfunction. Reid et al. (2014) have previously discussed that the modulation of metabolic pathways can affect seizure susceptibility. Taking this discussion into account, the comprehensive metabolic alterations evident from our data sets might actually contribute to epileptogenesis. In addition, PHC modules 3 and 7 comprised pathways related to mitochondrial function or to mitochondrial dysfunction. It is known that alterations in cell respiration and in the generation of reactive oxygen species can affect epileptogenesis (Rowley et al., 2015). Thus, this finding is in line with the already discussed association between mitochondrial dysfunction and epilepsy (Folbergrova and Kunz, 2012).

Protein interaction networks are characterized by a small number of highly connected protein nodes referred to as hub proteins (He and

Zhang, 2006). The majority of the significantly regulated top 5 hub proteins that we identified in our data set can be assigned to functional pathways discussed above. However, some hub proteins stand out from a functional point of view. These include synaptotagmin serving as a calcium sensor function thereby regulating neurotransmitter release (Jackman et al., 2016); H2A histone family member Y, a nuclear protein influencing nucleosome structure and regulating transcription (Hu et al., 2011) as well as different annexins playing a role in pro-inflammatory arachidonic acid signaling (Creutz et al., 2012). Several of these proteins including eukaryotic translation initiation factor 3 subunit C, H2A histone family member Y, hypoxia up-regulated 1, and transaldolase 1 have to our knowledge not been discussed in the context of epileptogenesis before.

Some of the intramodular hub proteins were also identified by PCA, such as, for instance, annexin A3. Junker et al. (2007) discussed a role for annexin A3 in apoptotic and phagocytotic processes in the brain. Thus, the detected upregulation in the latency phase, which was confirmed by immunohistochemistry, might be related to insult-triggered cell death.

On the first glimpse, hub proteins might serve as interesting target candidates based on their key switch function in the disease-associated protein-protein network. However, it needs to be considered that deletion of hub proteins has a higher probability to be lethal than deletion of a non-hub protein (He and Zhang, 2006). Thus, pharmacological targeting of hub proteins has a high potential for severe adverse effects and tolerability issues. Nevertheless, knowledge about hub proteins, their interactions and associated loops provides valuable information allowing integration of network biology in the design of module-based targeting approaches (Hopkins, 2008; Wang et al., 2012).

For comparative validation of the findings we have subjected a recently published data set to WGCNA analysis. The comparison revealed a partial overlap in enriched pathways characterizing identified modules and in hub proteins. These data provide first evidence for the robustness of our findings. The outcome of the comparison needs to consider that there are some similarities between the models regarding predictive validity. Both, the electrical and the chemical post-SE model have been described as models with difficult-to-treat or drug-resistant seizures (Löscher, 2011). On the other hand, there are huge differences in the experimental design of both studies and characteristics of the models, including the use of rats vs. mice, application of an electrical vs. chemical stimulus, requirement of electrode implantation vs. local injection, development of generalized tonic-clonic seizures vs. a mixture of non-convulsive electrographic seizures and behavioral convulsive seizures, and a week-long latency period vs. immediate epileptogenesis.

It is interesting to note that we observed an overlap in the network data despite these contrasting characteristics of the constructive and face validity of the models. This fact points to shared molecular pathophysiological mechanisms between the models, which might further confirm a comparable predictability regarding target and biomarker identification.

During the early post-insult phase and the latency phase PCA analysis of data from both brain regions revealed an obvious clustering also pointing to proteins that best distinguish between groups. The top protein lists contributing to dimension 1 might suggest biomarker candidates, which can serve as early molecular predictors of epileptogenesis following a brain insult. As mentioned in the introduction respective biomarkers might render a basis for molecular imaging approaches suitable for the identification of subgroups of patients at risk to develop epilepsy and for efficacy testing when evaluating anti-epileptogenic approaches. Thereby, proteins exhibiting a prominent upregulation should provide the most interesting candidates. Proteins, which as CD151 molecule proved to be overexpressed two days following SE, might be the most promising biomarkers for early risk assessment. It would be of particular interest to further study the regulation of CD151 molecule in more detail considering that CD151 molecule serves as a target for valproate and lithium in bipolar disorders (Hua et al., 2001) and that it might contribute to the regulation of blood-brain barrier tightness (Zhang et al., 2011). Proteins being up-regulated ten days following SE such as plexin B2 might provide a basis for follow-up and efficacy testing of intervention strategies. In contrast, proteins exhibiting a significant induction following onset of epilepsy might serve as a valuable basis for early diagnosis of epilepsy manifestation. Based on our analysis, molecular alterations in the PHC rather than those in the HC can provide a basis for respective epilepsy biomarkers.

As a major limitation of any molecular study with brain tissue sampling at early time points following an epileptogenic brain insult, we could only base our study design on the choice of a model in which animals reliably develop spontaneous seizures. It needs to be taken into account that invasive sampling does not allow to subsequently obtain information about the outcome regarding epilepsy development. The current study design of course does not allow to finally conclude whether a selected molecular alteration is associated with epileptogenesis or whether it merely reflects a consequence of the initial brain insult. Thus, it will be of utmost interest to assess whether biomarker candidates reliably predict epileptogenesis in a model with subgroups of animals with or without development of spontaneous recurrent seizures. This however, will only be feasible with a non-invasive assessment of the biomarker candidates e.g. by molecular imaging. The situation would of course be different with peripheral biomarkers from plasma or peripheral tissue as well as with cerebrospinal fluid sampling. Assessment of proteome alterations in respective samples should be further addressed in future studies. However, it needs to be taken into account that a sufficient number of proteins is necessary for a network analysis, which we have completed in the present study. The low number of proteins in CSF samples would therefore hamper this specific type of bioinformatics analysis.

Considering the outcome of the bioinformatics analysis it needs to be taken into account that databases used are based on a mixture of in vivo and in vitro data. With the currently available tools it is not possible to avoid a putative bias related to the fact that data obtained from an animal model are analysed based on these databases.

Moreover, data sets require validation by a focused analysis of selected proteins. Immunohistochemical analysis can thereby also provide additional information about the subregion specific and cellular distribution of differentially expressed proteins. In the present study, we confirmed an up-regulation of three selected proteins. These included annexin A3, which has already been discussed above, the chaperone protein clusterin, and eukaryotic translation initiation factor 3 subunit C. To our knowledge a regulation of the latter protein has not been discussed previously in the context of epileptogenesis. Eukaryotic translation initiation factor 3 subunit C, serves an essential function during the initiation of protein synthesis (Emmanuel et al., 2013). Silencing of its function can inhibit cell proliferation and promote apoptosis (Hao et al., 2015). It might be of interest to further study the role of this protein during epileptogenesis in more detail in future studies.

In conclusion, the first systems level analysis of proteome alterations during the course of epileptogenesis identified several modules of highly connected proteins in the HC and PHC. Characterization of the modules did not only further validate the data, but also revealed regulation of molecular processes not described previously in the context of epilepsy development. The data sets also provide valuable information about temporal patterns required for the development of preventive strategies.

In addition, PCA analysis suggests candidate biomarkers, which might inform the design of novel molecular imaging approaches aiming to predict epileptogenesis during different phases or to confirm epilepsy manifestation.

It is emphasized that the study design and the findings do not yet allow to distinguish between proteins that are undoubtedly linked with epileptogenesis and do not only reflect a molecular consequence of SE. Further studies with sequential molecular imaging in models

with subgroups with and without epilepsy development, will be crucial to provide relevant information about selected candidates. Moreover, application of network analysis to other models of epileptogenesis with different types of epileptogenic insults including models of traumatic brain injury or ischemia will provide data for comparison allowing the identification of key epileptogenesis proteins.

Acknowledgements

Research in Heidrun Potschka's group has been and is supported by grants of the Deutsche Forschungsgemeinschaft (DFG PO 681/5-2 and PO 681/8-1). The research performed by Ganna Androsova has received funding from the framework of the EU-funded FP7 (602461) research program BioCog (Biomarker Development for Postoperative Cognitive Impairment in the Elderly): www.biocog.eu. The authors thank Olga Cabezas, Marion Fisch, Sieglinde Fischlein, Barbara Kohler, Regina Rentsch and Angela Vicidomini for their excellent technical assistance.

The authors declare that they do not have any conflict of interest.

Appendix A. Supplementary data

Supplementary data to this article can be found online at http://dx.doi.org/10.1016/j.nbd.2017.05.017.

References

Albert, R., Jeong, H., Barabasi, A.L., 2000. Error and attack tolerance of complex networks. Nature 406, 378–382.
Benson, N., 2015. Network-based discovery through mechanistic systems biology. Implications for applications – SMEs and drug discovery: where the action is. Drug Discov. Today Technol. 15, 41–48.
Bitsika, V., Duveau, V., Simon-Areces, J., Mullen, W., Roucard, C., Makridakis, M., Mermelekas, G., Savvopoulos, P., Depaulis, A., Vlahou, A., 2016. High-throughput LC-MS/MS proteomic analysis of a mouse model of mesiotemporal lobe epilepsy predicts microglial activation underlying disease development. J. Proteome Res. 15, 1546–1562.
Brandt, C., Glien, M., Potschka, H., Volk, H., Loscher, W., 2003. Epileptogenesis and neuropathology after different types of status epilepticus induced by prolonged electrical stimulation of the basolateral amygdala in rats. Epilepsy Res. 55, 83–103.
Cairns, L., Tran, T., Kavran, J.M., 2017. Structural insights into the regulation of hippo signaling. ACS Chem. Biol. 12, 601–610.
Chin, J., Scharfman, H.E., 2013. Shared cognitive and behavioral impairments in epilepsy and Alzheimer's disease and potential underlying mechanisms. Epilepsy Behav. 26, 343–351.
Creutz, C.E., Hira, J.K., Gee, V.E., Eaton, J.M., 2012. Protection of the membrane permeability barrier by annexins. Biochemistry 51, 9966–9983.
Dijkstra, A.A., Ingrassia, A., de Menezes, R.X., Van Kesteren, R.E., Rozemuller, A.J., Heutink, P., Van de Berg, W.D., 2015. Evidence for immune response, axonal dysfunction and reduced endocytosis in the substantia Nigra in early stage Parkinson's disease. PLoS One 10, e0128651.
Dudek, F.E., Staley, K.J., 2011. The time course of acquired epilepsy: implications for therapeutic intervention to suppress epileptogenesis. Neurosci. Lett. 497, 240–246.
Emmanuel, R., Weinstein, S., Landesman-Milo, D., Peer, D., 2013. eIF3c: a potential therapeutic target for cancer. Cancer Lett. 336, 158–166.
Folbergrova, J., Kunz, W.S., 2012. Mitochondrial dysfunction in epilepsy. Mitochondrion 12, 35–40.
Galanopoulou, A.S., Gorter, J.A., Cepeda, C., 2012. Finding a better drug for epilepsy: the mTOR pathway as an antiepileptogenic target. Epilepsia 53, 1119–1130.
Gorter, J.A., Van Vliet, E.A., Aronica, E., Breit, T., Rauwerda, H., Lopes Da Silva, F.H., Wadman, W.J., 2006. Potential new antiepileptogenic targets indicated by microarray analysis in a rat model for temporal lobe epilepsy. J. Neurosci. 26, 11083–11110.
Gualtieri, F., Curia, G., Marinelli, C., Biagini, G., 2012. Increased perivascular laminin predicts damage to astrocytes in CA3 and piriform cortex following chemoconvulsive treatments. Neuroscience 218, 278–294.
Haanstra, J.R., Bakker, B.M., 2015. Drug target identification through systems biology. Drug Discov. Today Technol. 15, 17–22.
Hamosh, A., Scott, A.F., Amberger, J.S., Bocchini, C.A., Mckusick, V.A., 2005. Online Mendelian Inheritance in Man (OMIM), a knowledgebase of human genes and genetic disorders. Nucleic Acids Res. 33, D514–D517.
Hansen, K.F., Sakamoto, K., Pelz, C., Impey, S., Obrietan, K., 2014. Profiling status epilepticus-induced changes in hippocampal RNA expression using high-throughput RNA sequencing. Sci. Rep. 4, 6930.
Hao, J., Wang, Z., Wang, Y., Liang, Z., Zhang, X., Zhao, Z., Jiao, B., 2015. Eukaryotic initiation factor 3C silencing inhibits cell proliferation and promotes apoptosis in human glioma. Oncol. Rep. 33, 2954–2962.
Hauck, S.M., Dietter, J., Kramer, R.L., Hofmaier, F., Zipplies, J.K., Amann, B., Feuchtinger, A., Deeg, C.A., Ueffing, M., 2010. Deciphering membrane-associated molecular processes in target tissue of autoimmune uveitis by label-free quantitative mass spectrometry. Mol. Cell. Proteomics 9, 2292–2305.
Hauck, S.M., Hofmaier, F., Dietter, J., Swadzba, M.E., Blindert, M., Amann, B., Behler, J., Kremmer, E., Ueffing, M., Deeg, C.A., 2012. Label-free LC-MSMS analysis of vitreous from autoimmune uveitis reveals a significant decrease in secreted Wnt signalling inhibitors DKK3 and SFRP2. J. Proteome 75, 4545–4554.
He, X., Zhang, J., 2006. Why do hubs tend to be essential in protein networks? PLoS Genet. 2, e88.
He, K., Xiao, W., Lv, W., 2014. Comprehensive identification of essential pathways and transcription factors related to epilepsy by gene set enrichment analysis on microarray datasets. Int. J. Mol. Med. 34, 715–724.
Hopkins, A.L., 2008. Network pharmacology: the next paradigm in drug discovery. Nat. Chem. Biol. 4, 682–690.
Hu, Y., Chopra, V., Chopra, R., Locascio, J.J., Liao, Z., Ding, H., Zheng, B., Matson, W.R., Ferrante, R.J., Rosas, H.D., Hersch, S.M., Scherzer, C.R., 2011. Transcriptional modulator H2A histone family, member Y (H2AFY) marks Huntington disease activity in man and mouse. Proc. Natl. Acad. Sci. U. S. A. 108, 17141–17146.
Hua, L.V., Green, M., Wong, A., Warsh, J.J., Li, P.P., 2001. Tetraspan protein CD151: a common target of mood stabilizing drugs? Neuropsychopharmacology 25, 729–736.
Huang, J.Y., Tian, Y., Wang, H.J., Shen, H., Wang, H., Long, S., Liao, M.H., Liu, Z.R., Wang, Z.M., Li, D., Tao, R.R., Cui, T.T., Moriguchi, S., Fukunaga, K., Han, F., Lu, Y.M., 2016. Functional genomic analyses identify pathways dysregulated in animal model of autism. CNS Neurosci. Ther. 22, 845–853.
Jackman, S.L., Turecek, J., Belinsky, J.E., Regehr, W.G., 2016. The calcium sensor synaptotagmin 7 is required for synaptic facilitation. Nature 529, 88–91.
Jeong, H., Mason, S.P., Barabasi, A.L., Oltvai, Z.N., 2001. Lethality and centrality in protein networks. Nature 411, 41–42.
Jessberger, S., Parent, J.M., 2015. Epilepsy and adult neurogenesis. Cold Spring Harb. Perspect. Biol. 7.
de Jong, S., Boks, M.P., Fuller, T.F., Strengman, E., Janson, E., de Kovel, C.G., Ori, A.P., Vi, N., Mulder, F., Blom, J.D., Glenthoj, B., Schubart, C.D., Cahn, W., Kahn, R.S., Horvath, S., Ophoff, R.A., 2012. A gene co-expression network in whole blood of schizophrenia patients is independent of antipsychotic-use and enriched for brain-expressed genes. PLoS One 7, e39498.
Junker, H., Suofu, Y., Venz, S., Sascau, M., Herndon, J.G., Kessler, C., Walther, R., Popa-Wagner, A., 2007. Proteomic identification of an upregulated isoform of annexin A3 in the rat brain following reversible cerebral ischemia. Glia 55, 1630–1637.
Kassambara, A., 2015. Factoextra: visualization of the outputs of a multivariate analysis. R package version, 1.
Kobow, K., Auvin, S., Jensen, F., Loscher, W., Mody, I., Potschka, H., Prince, D., Sierra, A., Simonato, M., Pitkanen, A., Nehlig, A., Rho, J.M., 2012. Finding a better drug for epilepsy: antiepileptogenesis targets. Epilepsia 53, 1868–1876.
Langfelder, P., Horvath, S., 2008. WGCNA: an R package for weighted correlation network analysis. BMC Bioinf. 9, 559.
Lê, S., Josse, J., Husson, F., 2008. FactoMineR: an R package for multivariate analysis. J. Stat. Softw. 25, 1–18.
Lee, T.S., Mane, S., Eid, T., Zhao, H., Lin, A., Guan, Z., Kim, J.H., Schweitzer, J., King-Stevens, D., Weber, P., Spencer, S.S., Spencer, D.D., De Lanerolle, N.C., 2007. Gene expression in temporal lobe epilepsy is consistent with increased release of glutamate by astrocytes. Mol. Med. 13, 1–13.
Löscher, W., 2011. Critical review of current animal models of seizures and epilepsy used in the discovery and development of new antiepileptic drugs. Seizure 20, 359–368.
Löscher, W., Klitgaard, H., Twyman, R.E., Schmidt, D., 2013. New avenues for anti-epileptic drug discovery and development. Nat. Rev. Drug Discov. 12, 757–776.
Margineanu, D.G., 2016. Neuropharmacology beyond reductionism - a likely prospect. Biosystems 141, 1–9.
Miller, J.A., Horvath, S., Geschwind, D.H., 2010. Divergence of human and mouse brain transcriptome highlights Alzheimer disease pathways. Proc. Natl. Acad. Sci. U. S. A. 107, 12698–12703.
Niesen, C.E., Xu, J., Fan, X., Li, X., Wheeler, C.J., Mamelak, A.N., Wang, C., 2013. Transcriptomic profiling of human peritumoral neocortex tissues revealed genes possibly involved in tumor-induced epilepsy. PLoS One 8, e56077.
Noebels, J., 2011. A perfect storm: converging paths of epilepsy and Alzheimer's dementia intersect in the hippocampal formation. Epilepsia 52 (Suppl. 1), 39–46.
Okamoto, O.K., Janjoppi, L., Bonone, F.M., Pansani, A.P., Da Silva, A.V., Scorza, F.A., Cavalheiro, E.A., 2010. Whole transcriptome analysis of the hippocampus: toward a molecular portrait of epileptogenesis. BMC Genomics 11, 230.
Ongerth, T., Russmann, V., Fischborn, S., Boes, K., Siegl, C., Potschka, H., 2014. Targeting of microglial KCa3.1 channels by TRAM-34 exacerbates hippocampal neurodegeneration and does not affect ictogenesis and epileptogenesis in chronic temporal lobe epilepsy models. Eur. J. Pharmacol. 740, 72–80.
Paxinos, G., Watson, C., 2007. The Rat Brain in Stereotaxic Coordinates. sixth ed. Academic Press, Elsevier, San Diego, California.
Pekcec, A., Fuest, C., Muhlenhoff, M., Gerardy-Schahn, R., Potschka, H., 2008. Targeting epileptogenesis-associated induction of neurogenesis by enzymatic depolysialylation of NCAM counteracts spatial learning dysfunction but fails to impact epilepsy development. J. Neurochem. 105, 389–400.
Pinero, J., Queralt-Rosinach, N., Bravo, A., Deu-Pons, J., Bauer-Mehren, A., Baron, M., Sanz, F., Furlong, L.I., 2015. DisGeNET: a discovery platform for the dynamical exploration of human diseases and their genes. Database (Oxf.) 2015, bav028.
Pitkänen, A., Nissinen, J., Nairismagi, J., Lukasiuk, K., Grohn, O.H., Miettinen, R., Kauppinen, R., 2002. Progression of neuronal damage after status epilepticus and during spontaneous seizures in a rat model of temporal lobe epilepsy. Prog. Brain Res. 135, 67–83.
Potschka, H., Brodie, M.J., 2012. Pharmacoresistance. Handb. Clin. Neurol. 108, 741–757.
Racine, J., Gerber, V., Feutz, M.M., Riley, C.P., Adamec, J., Swinburne, J.E., Couetil, L.L., 2011. Comparison of genomic and proteomic data in recurrent airway obstruction affected horses using Ingenuity Pathway Analysis(R). BMC Vet. Res. 7, 48.

Reid, C.A., Mullen, S., Kim, T.H., Petrou, S., 2014. Epilepsy, energy deficiency and new therapeutic approaches including diet. Pharmacol. Ther. 144, 192–201.
Ren, F., Zhang, L., Jiang, J., 2010. Hippo signaling regulates Yorkie nuclear localization and activity through 14-3-3 dependent and independent mechanisms. Dev. Biol. 337, 303–312.
Ren, Y., Cui, Y., Li, X., Wang, B., Na, L., Shi, J., Wang, L., Qiu, L., Zhang, K., Liu, G., Xu, Y., 2015. A co-expression network analysis reveals lncRNA abnormalities in peripheral blood in early-onset schizophrenia. Prog. Neuro-Psychopharmacol. Biol. Psychiatry 63, 1–5.
Rowley, S., Liang, L.P., Fulton, R., Shimizu, T., Day, B., Patel, M., 2015. Mitochondrial respiration deficits driven by reactive oxygen species in experimental temporal lobe epilepsy. Neurobiol. Dis. 75, 151–158.
Schindler, C.K., Heverin, M., Henshall, D.C., 2006. Isoform- and subcellular fraction-specific differences in hippocampal 14-3-3 levels following experimentally evoked seizures and in human temporal lobe epilepsy. J. Neurochem. 99, 561–569.
Schmidt, D., 2012. Is antiepileptogenesis a realistic goal in clinical trials? Concerns and new horizons. Epileptic Disord. 14, 105–113.
Shannon, P., Markiel, A., Ozier, O., Baliga, N.S., Wang, J.T., Ramage, D., Amin, N., Schwikowski, B., Ideker, T., 2003. Cytoscape: a software environment for integrated models of biomolecular interaction networks. Genome Res. 13, 2498–2504.
Shirasaki, D.I., Greiner, E.R., Al-Ramahi, I., Gray, M., Boontheung, P., Geschwind, D.H., Botas, J., Coppola, G., Horvath, S., Loo, J.A., Yang, X.W., 2012. Network organization of the huntingtin proteomic interactome in mammalian brain. Neuron 75, 41–57.
Smyth, G.K., 2004. Linear models and empirical bayes methods for assessing differential expression in microarray experiments. Stat. Appl. Genet. Mol. Biol. 3 Article3.
Stam, C.J., Jones, B.F., Nolte, G., Breakspear, M., Scheltens, P., 2007. Small-world networks and functional connectivity in Alzheimer's disease. Cereb. Cortex 17, 92–99.
Tan, N., Chung, M.K., Smith, J.D., Hsu, J., Serre, D., Newton, D.W., Castel, L., Soltesz, E., Pettersson, G., Gillinov, A.M., Van Wagoner, D.R., Barnard, J., 2013. Weighted gene coexpression network analysis of human left atrial tissue identifies gene modules associated with atrial fibrillation. Circ. Cardiovasc. Genet. 6, 362–371.
Trinka, E., Brigo, F., 2014. Antiepileptogenesis in humans: disappointing clinical evidence and ways to move forward. Curr. Opin. Neurol. 27, 227–235.
Vezzani, A., 2012. Before epilepsy unfolds: finding the epileptogenesis switch. Nat. Med. 18, 1626–1627.
Walker, A., Russmann, V., Deeg, C.A., Von Toerne, C., Kleinwort, K.J., Szober, C., Rettenbeck, M.L., Von Ruden, E.L., Goc, J., Ongerth, T., Boes, K., Salvamoser, J.D., Vezzani, A., Hauck, S.M., Potschka, H., 2016. Proteomic profiling of epileptogenesis in a rat model: focus on inflammation. Brain Behav. Immun. 53, 138–158.
Wang, Z., Liu, J., Yu, Y., Chen, Y., Wang, Y., 2012. Modular pharmacology: the next paradigm in drug discovery. Expert Opin. Drug Discovery 7, 667–677.
White, H.S., 2012. Animal models for evaluating antiepileptogenesis. In: Noebels, J.L., Avoli, M., Rogawski, M.A., Olsen, R.W., Delgado-Escueta, A.V. (Eds.), Jasper's Basic Mechanisms of the Epilepsies, fourth ed. National Center for Biotechnology Information (US), Bethesda (MD).
Zack, G.W., Rogers, W.E., Latt, S.A., 1977. Automatic measurement of sister chromatid exchange frequency. J. Histochem. Cytochem. 25, 741–753.
Zhang, F., Michaelson, J.E., Moshiach, S., Sachs, N., Zhao, W., Sun, Y., Sonnenberg, A., Lahti, J.M., Huang, H., Zhang, X.A., 2011. Tetraspanin CD151 maintains vascular stability by balancing the forces of cell adhesion and cytoskeletal tension. Blood 118, 4274–4284.
Zhang, H., Geng, D., Gao, J., Qi, Y., Shi, Y., Wang, Y., Jiang, Y., Zhang, Y., Fu, J., Dong, Y., Gao, S., Yu, R., Zhou, X., 2016. Expression and significance of Hippo/YAP signaling in glioma progression. Tumour Biol. 37, 15665–15676.